Mineralogical Magazine, October 2017, Vol. 81(5), pp. 1261–1277

Cancrinite–vishnevite solid solution from Cinder Lake (Manitoba, Canada): crystal chemistry and implications for alkaline igneous rocks

Tânia Martins[1*], Ryan Kressall[2], Luca Medici[3] and Anton R. Chakhmouradian[4]

[1] Manitoba Geological Survey, 360-1395 Ellice Avenue, Winnipeg, Manitoba R3G 3P2, Canada
[2] Department of Earth Sciences, Dalhousie University, 1355 Oxford Street, Halifax, Nova Scotia B3H 4R2, Canada
[3] CNR – Istituto di Metodologie per l'Analisi Ambientale, Tito Scalo, I–85050 Potenza, Italy
[4] Department of Geological Sciences, University of Manitoba, 125 Dysart Road, Winnipeg, Manitoba R3T 2N2, Canada

[*Received 29 August 2016; Accepted 28 October 2016; Associate Editor: Giancarlo Della Ventura*]

ABSTRACT

This paper presents a microbeam (electron microprobe, Raman spectroscopic and X-ray microdiffraction) study of cancrinite-group minerals of relevance to alkaline igneous rocks. A solid solution is known to exist between cancrinite and vishnevite with the principal substitutions being CO_3^{2-} by SO_4^{2-} and Ca for Na. In the present study, several intermediate members of the cancrinite–vishnevite series from a syenitic intrusion at Cinder Lake (Manitoba, Canada), were used to examine how chemical variations in this series affect their spectroscopic and structural characteristics. The Cinder Lake samples deviate from the ideal cancrinite–vishnevite binary owing to the presence of cation vacancies. The only substituent elements detectable by electron microprobe are K, Sr and Fe (0.03–0.70, 0–0.85 and 0–0.45 wt.% respective oxides). The following Raman bands are present in the spectra of these minerals: ~631 cm^{-1} and ~984–986 cm^{-1} [SO_4^{2-} vibration modes]; ~720–774 cm^{-1} and ~1045–1060 cm^{-1} [CO_3^{2-} vibration modes]; and ~3540 cm^{-1} and 3591 cm^{-1} [H_2O vibration modes]. Our study shows a clear relationship between the chemical composition and Raman characteristics of intermediate members of the cancrinite–vishnevite series, especially with regard to stretching modes of the CO_3^{2-} and SO_4^{2-} anions. From cancrinite-poor ($Ccn_{6.5}$) to cancrinite-dominant ($Ccn_{91.3}$) compositions, the SO_4^{2-} vibration modes disappear from the Raman spectrum, giving way to CO_3^{2-} modes. X-ray microdiffraction results show a decrease in unit-cell parameters towards cancrinite-dominant compositions: $a = 12.664$ (1) Å, $c = 5.173$(1) Å for vishnevite (Ccn_{22}); $a = 12.613$ (1) Å, $c = 5.132$(1) Å for cancrinite (Ccn_{71}). Our results demonstrate that Raman spectroscopy and X-ray microdiffraction are effective for *in situ* identification of microscopic grains of cancrinite–vishnevite where other methods (e.g. infrared spectroscopy) are inapplicable. The petrogenetic implications of cancrinite–vishnevite relations for tracing early- to late-stage evolution of alkaline magmas are discussed.

Keywords: cancrinite, vishnevite, feldspathoid syenite, alkaline igneous rocks, Raman spectroscopy, X-ray microdiffraction, Cinder Lake, Manitoba.

Introduction

Cancrinite-group minerals are hexagonal framework aluminosilicates with a zeolite-like structure that consists of chains of cages and adjacent channels which run parallel to the *c* axis (Grundy and Hassan, 1982, Hassan and Grundy, 1984; Hassan and Buseck, 1992). Cages and channels can be occupied by cations (Na^+, Ca^{2+}, K^+), anions [$(CO_3)^{2-}$, $(SO_4)^{2-}$, OH^- and Cl^-) and molecular species (mainly H_2O, Grundy and Hassan, 1982; and CO_2, Della Ventura and Bellatreccia, 2004;

*E-mail: tania.martins@gov.mb.ca
https://doi.org/10.1180/minmag.2016.080.165

Della Ventura *et al*., 2005). Due to their chemical properties, structure and thermal stability (Hassan 1996*a*,*b*; Hassan *et al*., 2006; Gatta *et al*., 2014), they have potential for a wide array of applications in technology and industry. For example, cancrinite-structured materials have been proposed as storage matrices for alkaline wastes (Gatta and Lotti, 2016) and in high-level nuclear waste treatment (Barney, 1976). Upon heating at ambient pressure, cancrinite dehydrates at 748 K, and the dehydrated form is stable up to 823 K (Gatta *et al*., 2014). At ambient temperatures, cancrinite-group members are stable to pressures in excess of 5 GPa (Gatta and Lee, 2008; Lotti *et al*., 2012, 2014*a*,*b*; Gatta and Lotti, 2016), which is surprising for a microporous structure. Other studies showed that cancrinite and related phases are sensitive to variations in CO_2 activity in natural systems (Pekov *et al*., 2011), thus representing a potentially valuable petrogenetic indicator for alkaline igneous rocks (see below).

Complete chemical analyses of cancrinite-group feldspathoids are difficult to obtain due to the presence of different extra-framework anions, cations and molecular species undetectable by electron microprobe analysis (Della Ventura and Bellatreccia, 2004; Della Ventura *et al*., 2005, 2008; Hassan and Grundy, 1991). Vibrational spectroscopic techniques are becoming increasingly popular for the study of minerals containing H_2O, CO_2 (Della Ventura *et al*., 2009) or other components that cannot be quantified by electron microprobe, but there are relatively few such studies applicable to petrological problems. Previously, cancrinite and related minerals were investigated by infrared spectroscopy (Rastsvetaeva *et al*., 2007; Della Ventura *et al*., 2007, Chukanov *et al*., 2011), but this technique is not applicable to microscopic (1–30 μm) mineral grains in polished thin sections and, as such, is of limited use in igneous petrology. Very few studies have focused on the Raman spectroscopy of cancrinite and related phases. Raman spectra of near end-member natural cancrinite and vishnevite were examined by Reshetnyak *et al*. (1988). Gatta *et al*. (2012) presented data for natural cancrinite from an unspecified locality in Cameroon, and a spectrum of cancrinite replacing nepheline in the Oktiabrski massif (Ukraine) was reported by Dumańska-Słowik *et al*. (2016).

In the present work, we identified a continuous series of compositions spanning most of the cancrinite–vishnevite solid solution range in a suite of feldspathoid syenites from Cinder Lake, Manitoba, Canada. These phases are abundant throughout the host syenite and occur in grain sizes amenable to *in situ* microbeam analysis, providing a unique opportunity to study variations in their structural and spectroscopic characteristics over a wide range of compositions. In this contribution, we demonstrate that Raman spectroscopy is an extremely useful non-destructive *in situ* technique that can be used to accurately identify extra-framework species in cancrinite-group feldspathoids.

Background information

Cancrinite $[(Na,Ca)_6(CO_3)_{1.4–1.7}][NaH_2O]_2[Al_6Si_6O_{24}]$ and vishnevite $[(Na,K)_6(SO_4)][NaH_2O]_2[Al_6Si_6O_{24}]$ are petrologically important feldspathoid minerals and the two most common members of the cancrinite (-davyne) group, which consists of >20 hexagonal framework aluminosilicates with additional anions (typically, carbonate, sulfate and chloride). Cancrinite and vishnevite form a complete solid solution characterized principally by the coupled substitution $2Ca^{2+} + 2CO_3^{2-} \leftrightarrow 2Na^+ + SO_4^{2-}$, although other substitutions in the Na and anion sites are also common. In cancrinite and vishnevite, the Na1 site is in the 6R windows shared by the cancrinitic cages along [0001], and always occupied by Na^+ atoms. All the substitutions involving Na^+, Ca^{2+}, K^+, Sr^{2+} or vacancies occur only in the Na2 site, which is off-centred within the channels. Anions such as CO_3^{2-}, SO_4^{2-} and OH^- are located in the channels (Grundy and Hassan, 1982; Hassan and Grundy, 1991), while Cl^- and H_2O groups sit in the cancrinitic cages. The sulfate ion does not replace CO_3^{2-} on a 1:1 basis. Instead, it has been observed that carbonate-rich members tend to have a greater proportion of $SO_4^{2-} + CO_3^{2-}$ anions than vishnevite-dominant members of the series (Deer *et al*., 1992). Potassium has been identified as a common substituent element in the alkali sites within the channels, and the stoichiometry of the aluminosilicate framework has been shown to depart from the ideal proportions towards Si-rich compositions (Pekov *et al*., 2011). A simplified general formula for this mineral series could thus be written as $(Na,Ca,K)_{6–8}Al_{6–x}Si_{6+x}O_{24}(CO_3,SO_4,Cl,OH)_{1–2}\cdot nH_2O$, where x is typically << 1 and n = 1–5.

Cancrinite-group minerals commonly occur in silica-undersaturated rocks (syenites and ijolite–urtite series) either as a primary phase precipitated from evolved volatile-rich magmas, or as a product of reaction between primary nepheline and volatile-rich melts or fluids (Deer *et al*., 1992). Cancrinite and

https://doi.org/10.1180/minmag.2016.080.165 Published online by Cambridge University Press

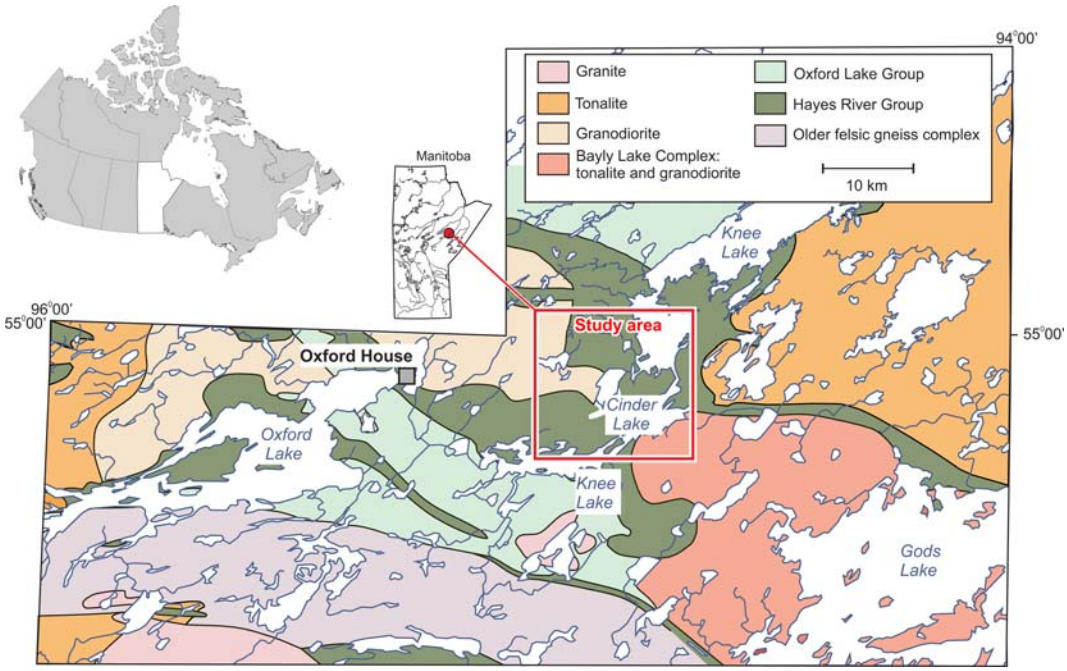

FIG. 1. Geographic location and simplified regional geology of the Cinder Lake area; assembled on the basis of the Manitoba Geological Survey 1:1,000,000 geological maps.

vishnevite have been recognized at numerous localities around the world (Pekov *et al*., 2011), but the best-studied examples are those from Laacher See, Eifel, Germany (Chukanov *et al*., 2011; Pekov *et al*., 2011); Loch Borralan, Scotland and Latium, Italy (Della Ventura *et al*., 2007); Ilmeny and Vishnevye Mountains, Urals, Russia (Hassan and Grundy, 1984; Della Ventura *et al*., 2007; Chukanov *et al*., 2011; Pekov *et al*., 2011); Dakhunur and Bayankol, Tuva, Russia (Reshetnyak *et al*., 1988); Kovdor, Khibiny and Lovozero, Kola Peninsula, Russia (Rastsvetaeva *et al*., 2007; Olysych *et al*., 2008); and Tamazert, High Atlas, Morocco (Chukanov *et al*., 2011; Pekov *et al*., 2011). In Canada, cancrinite was reported from biotite-nepheline gneisses of the Bancroft area (Phoenix and Nuffield, 1949), where one of the collecting sites is colloquially known as the Cancrinite Hill, and sodalite syenites of Mont Saint-Hilaire (Horváth and Gault, 1990), but no detailed studies of any Canadian material have been published.

Geological setting

We identified members of the cancrinite–vishnevite series in an alkaline intrusion of Archean age in the NW part of the Superior craton, eastern Manitoba. The intrusion, known as the Cinder Lake alkaline complex, is located within the greenstone belt of the Oxford Lake and Knee Lake, which is part of the Oxford–Stull domain of the Superior province (Stott *et al*., 2010; Fig. 1). Supracrustal rocks in this greenstone belt include the older basalt-dominant Hayes River Group and the younger more compositionally diverse Oxford Lake Group (division and nomenclature introduced by Wright, 1932). The Hayes River Group is mainly composed of pillow basalt and gabbro with subordinate intermediate and felsic volcanic-sedimentary rocks (Gilbert, 1985; Hubregtse, 1985), which have been radiometrically dated at 2.83 Ga (Corkery *et al*., 2000). The Bayly Lake plutonic complex intrudes the Hayes River Group (2.78 and 2.73 Ga; Corkery *et al*., 2000) and varies from tonalite to granite in composition. The Oxford Lake Group, which consists of a lower, ~2.72 Ga, volcanic subgroup and an upper, ~2.71 Ga, subaerial to shallow-marine sedimentary subgroup, is separated from the Hayes River Group and Bayly Lake plutonic complex by an unconformity (Corkery *et al*., 2000). The Oxford Lake Group is also intruded by tonalite–granodiorite–granite plutons, with a minimum age constrained by the Magill

https://doi.org/10.1180/minmag.2016.080.165 Published online by Cambridge University Press

Lake pluton south of Knee Lake (2668 ±1 Ma; Lin *et al*., 2006). The Cinder Lake complex comprises a wide variety of igneous and variably metasomatized igneous rocks, including feldspathoid syenites. It is emplaced into the Hayes River Group mafic sequence, and was radiometrically dated at 2705 Ma (Chakhmouradian *et al*., 2008).

Kressall (2012) defined the exposures of the alkaline intrusive complex at Cinder Lake as comprising a suite of syenitic rocks, thought to represent the main component of the complex, and a monzogranite pluton that outcrops in the centre and towards the northwestern corner of the lake. Among the granitic rocks, the most common type is pink, massive, medium-grained monzogranite. It is composed mostly of plagioclase, quartz and microcline with accessory hornblende (commonly altered to epidote), phlogopite, magnetite, titanite, apatite and zircon. This rock is metasomatized close to the alkaline intrusive complex, with intergrown microcline, albite, diopside and minor interstitial quartz, apatite, titanite and magnetite as inclusions in diopside. Larger apatite crystals (up to 1 mm long) are present in association with andradite and Fe-(hydro) oxide veinlets. The syenitic suite can be subdivided into four main units (Kressall, 2012): pegmatoid alkali-feldspar syenite; cancrinite-nepheline syenite; and vishnevite syenite with spatially associated minor porphyritic cancrinite syenite.

Petrography

The present work was focused on feldspathoid syenites forming limited outcrops in the SE part of the lake and a few islands on the lake itself. The fine-grained mesocratic-to-leucocratic cancrinite-nepheline syenite consists mainly of small clinopyroxene prisms set in a groundmass of anhedral microcline and nepheline partially replaced by albite and cancrinite, respectively (Figs 2*a*,*b*). Locally, secondary muscovite, natrolite and minor stronalsite also occur in association with cancrinite, albite, minor calcite and allanite. Other accessory minerals include phlogopite, titanite, magnetite, apatite, monazite, britholite and thorite. The vishnevite syenite is composed of subhedral to euhedral, flow-aligned microcline laths set in a very fine-grained mosaic of vishnevite, albite, calcite and abundant platy phlogopite crystals (Fig. 2*c*). It differs from the cancrinite-nepheline syenite by the absence of nepheline, and the presence of vishnevite, minor sodalite and fluorite. Other accessory constituents are pyrite, aegirine, magnetite, apatite, allanite, zircon and celestine. Pyrrhotite is characteristically absent.

In these rocks, cancrinite occurs as a primary late-stage major constituent interstitial with respect to feldspars and biotite (Fig. 2*d*), or as a secondary mineral replacing nepheline (Fig. 2*b*, *e*). Vishnevite occurs interstitially to calcite, potassium feldspar and biotite (Fig. 2*c*); leucocratic microcline-vishnevite-calcite ocelli were observed in one melasyenite outcrop (Fig. 2*f*). Cancrinite is recognizable under crossed polars by its upper first-order to lower second-order interference colours ($\delta \leq 0.025$), but its birefringence decreases with increasing proportions of vishnevite. Vishnevite shows first-order interference colours ($\delta = 0.005$–0.015) and may be easily confused with nepheline (also uniaxial negative) or feldspars if not in an optic axis orientation. Clearly, birefringence measurements are not a reliable means of discriminating between cancrinite and vishnevite.

Methodology

All analytical measurements were performed *in situ* on representative syenite samples containing minerals of the cancrinite–vishnevite series chosen through careful petrographic examination of polished thin sections. For consistency, grain sections oriented perpendicular to the optic axis [0001] were selected for further examination, wherever possible. The composition of all minerals was determined by wavelength dispersive X-ray spectrometry (WDS) using a Cameca SX100 electron-microprobe operated at an accelerating voltage of 15 kV and a beam current of 10 nA. These analyses were carried out using a beam defocused to 20 μm to minimize the loss or diffusion of alkalis and halogens. The following standards were employed for the analysis: albite (Na), orthoclase (K), diopside (Ca and Si), $SrTiO_3$ (Sr), andalusite (Al), fayalite (Fe), tugtupite (Cl) and barite (S). The peak and background counting times were 20 and 10 s, respectively, for all elements. The raw data were reduced and corrected using the "*PAP*" method of Pouchou and Pichoir (1985).

Raman spectra were recorded using a LabRAM ARAMIS system (HORIBA Jobin-Yvon) equipped with an electronically cooled multichannel charge-coupled device detector, interfaced with *LabSpec5* software. A He-Ne laser emitting at 633 nm with a nominal output power of 50 mW (CVI Melles Griot) was chosen as the excitation source. The use of a lower wavelength (e.g. 532 nm) source was

https://doi.org/10.1180/minmag.2016.080.165 Published online by Cambridge University Press

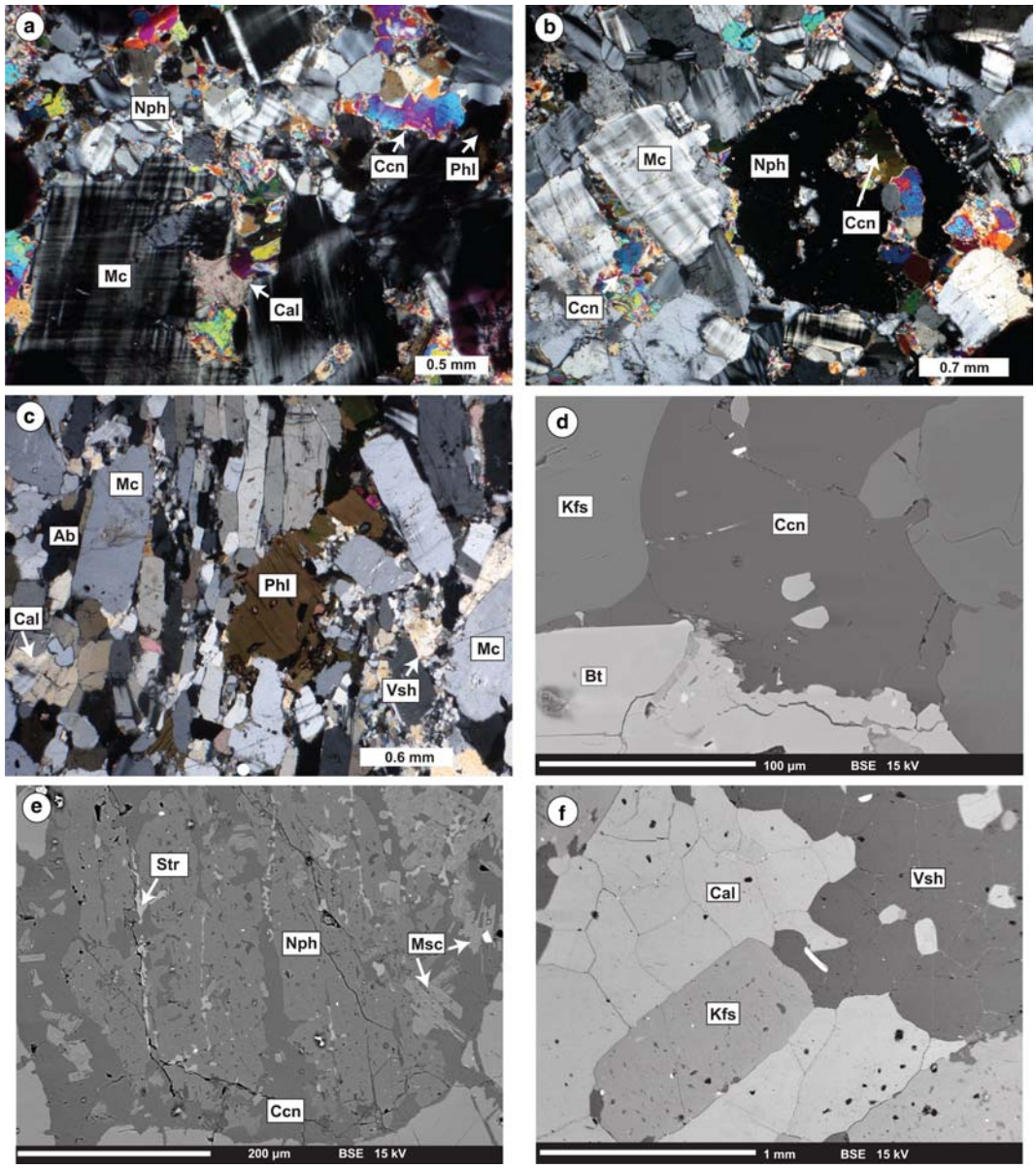

FIG. 2. Microphotographs and back-scattered electron (BSE) images of cancrinite-group minerals from Cinder Lake. (*a*) Groundmass interstitial primary cancrinite (Ccn) associated with microcline (Mc), nepheline (Nph), calcite (Cal) and phlogopite (Phl) (cancrinite-nepheline syenite, sample 03-01, crossed nicols); (*b*) resorbed nepheline crystals partially replaced by cancrinite (cancrinite-nepheline syenite, sample 08-01, crossed nicols); (*c*) trachytoidal texture in vishnevite (Vsh) syenite (sample 12-04, crossed nicols); (*d*) cancrinite occurring interstitially to biotite (Bt) and potassium feldspar (Kfs) in cancrinite-nepheline syenite (sample 07-01; BSE image); (*e*) stronalsite (Str) and muscovite (Msc) associated with cancrinite after nepheline in cancrinite-nepheline syenite (sample 08-08-01; BSE image); (*f*) vishnevite occurring in association with calcite and K-feldspar in leucocratic ocelli within vishnevite syenite (sample 04-01; BSE image).

https://doi.org/10.1180/minmag.2016.080.165 Published online by Cambridge University Press

precluded by fluorescence in vishnevite. The beam was focused to ~2 μm using an Olympus ×100 objective, and spectra acquired in confocal mode at room temperature. Spectra were collected with a diffraction grating of 1800 grooves mm^{-1} and other instrumental parameters (data collection times, slit width, etc.) were optimized by performing multiple measurements on the same area. The spectrometer was calibrated using a polished silicon wafer as a standard for the 520.7 cm^{-1} calibration line. A curve fitting technique applying the Gaussian function was used to determine the Raman shift of characteristic vibration modes.

X-ray microdiffraction (μXRD) data were collected *in situ* using a Rigaku D/MAX RAPID diffraction system operated at 40 kV and 30 mA. This instrument is equipped with a Cu$K\alpha$ source, curved image plate detector, flat graphite monochromator, a variety of beam collimators, motorized stage and microscope for accurate positioning of the sample. The motorized stage allows two angular movements (rotation and revolution). Data were collected in reflection mode using various sample-to-beam geometries and operating conditions. For samples 03-01, 08-01 and 04-01, the datasets were obtained over a 16 h period using a 0.05 mm collimator with a fixed ω angle and a Φ rotation range of 360°. Samples 12-02, 12-05 and additional grains in sample 04-01 required two data collection cycles, each with a 0.05 mm collimator, 8 h collection time, fixed ω angle and a Φ rotation range of 180° (the sum of the two collections yielding the complete 360° coverage). A complete dataset for sample 12-05 required five measurements, each one with a 0.05 mm collimator and a collection time of 2 h. The ω angle was fixed and Φ rotation ranges of 20°, 40°, 50°, 80° and 170° (their sum yielding the 360° coverage) were used. The geometric features of the instrument, the dimensions of the thin sections, and the positions of the points analysed limited the grazing incidence angles of the X-ray beam, resulting in the loss of diffraction signals with $2\theta < 18°$. The μXRD data were collected as two-dimensional images and then converted into 2θ–*I* profiles using Rigaku *R-Axis Display* software. Unit-cell parameters were refined using *UnitCell* software (Holland and Redfern, 1997).

Results

Chemical composition

Because the CO_2 content of the samples studied could not be quantified, but element correlations and spectroscopic data indicate the presence of carbonate in these minerals (see below), we used charge considerations to calculate the proportion of this component in our samples: CO_3^{2-} pfu = ($\Sigma Sq^+ - 48 - 2 \times S$ apfu)/2, where ΣSq^+ is the total positive charge contributed by cations and (a)pfu stands for (atoms) per formula unit. Assuming the end-member formula $Na_6Ca_2(Al_6Si_6O_{24})(CO_3)_2 \cdot nH_2O$, the proportion of cancrinite is then calculated as Ccn = $50 \times CO_3^{2-}/[0.5 \times CO_3^{2-} + SO_4^{2-}]$. End-member cancrinite and vishnevite were not observed in the Cinder Lake samples; all analyses contain some proportion of both end-member components, and span from ~Ccn_3Vsh_{97} to $Ccn_{95}Vsh_5$ (Table 1).

Analysed samples when plotted in the discrimination diagram of Hassan and Grundy (1984), our Fig. 3, fall within the field of non-stoichiometric compositions and cover nearly the entire series. The highest value of S (7.4 wt.% SO_3) was observed in sample 04-01. The measured SO_4^{2-} and calculated CO_3^{2-} contents are strongly correlated with Ca + Sr rather than Na (Fig. 4*a*,*b*), in agreement with published data from other localities (Pekov *et al*., 2011). One notable exception is sample 07-01 in the interval between 0.82 and 0.87 Ca apfu, where SO_4^{2-} concentrations deviate from the otherwise linear trend towards lower values (0.3–0.4 *vs.* the expected 0.5–0.6 SO_4^{2-} pfu). The most plausible explanation for this discrepancy is that OH^- or another undetected channel species is present in this phase, resulting in the overestimated carbonate content. An intermediate member of the cancrinite–hydroxycancrinite series has been reported by Chukanov *et al*. (2011), but conclusive identification of such phases is impossible in the absence of infrared data.

The total number of cations in the large cation sites in the recalculated formulae varies from 7.28 to 7.86 apfu, consistently lower than the ideal value of 8. This is probably due to vacancies in these sites. Low cation totals similar to those in Table 1 are not uncommon (Hassan and Grundy, 1984; Rastsvetaeva *et al*., 2007; Pekov *et al*., 2011). In terms of the Si:Al ratio, the samples range from 1.06 to 1.01, with the widest variations observed in vishnevite-dominant compositions. Calcium varies from 0.3 to 1.5 apfu, well within the range reported in the literature for both cancrinite and vishnevite (Pekov *et al*., 2011), with the highest Ca values seen in cancrinite-rich members. Potassium is most abundant (0.4–0.7 wt.% K_2O) in Na-rich samples close to the vishnevite end-member, whereas compositions with ≥40% Ccn contain negligible

https://doi.org/10.1180/minmag.2016.080.165 Published online by Cambridge University Press

TABLE 1. Major-element compositions of cancrinite-group minerals from Cinder Lake (arranged in order of decreasing SO_3 content).

Rock type	Vsh sye (leucocratic lenses)		Vsh sye		Vsh sye (trachytoidal texture)				Porphyritic cancrinite syenite				
Sample no.	04-01		03-02	03-02	12-02		12-02		12-05	12-05		12-05	
Orientation	⊥ *c* axis		RO	RO	⊥ *c* axis		RO		RO	RO		⊥ *c* axis	
Na_2O (wt.%)	21.46	20.62	19.89	19.82	20.37	20.02	19.93	20.64	19.08	18.92	19.41	19.55	19.45
Al_2O_3	29.26	29.01	29.07	27.93	29.36	29.42	28.78	29.02	28.58	28.55	29.03	29.3	29.26
SiO_2	36.05	35.92	34.70	34.91	35.60	35.34	34.25	34.87	34.04	34.52	35.29	35.62	34.97
SO_3	6.94	6.80	5.76	5.59	4.30	4.25	4.10	4.25	3.37	3.24	3.48	3.32	3.45
K_2O	0.57	0.62	0.40	0.70	0.12	0.12	0.12	0.12	0.07	0.07	0.08	0.08	0.06
CaO	2.10	2.00	3.39	3.31	4.51	4.45	4.35	4.45	5.44	5.45	5.49	5.52	5.50
Fe_2O_3	n.d.	0.45	n.d.	0.15	n.d.	n.d.	n.d.	n.d.	0.05	0.21	0.02	n.d.	0.02
SrO	0.31	0.32	0.35	0.4	0.68	0.49	0.58	0.51	0.27	0.33	0.30	0.35	0.39
Total	96.69	95.74	93.56	92.81	94.94	94.09	92.11	93.86	90.90	91.29	93.10	93.74	93.10
Mineral formulae calculated on the basis of 12 Si + Al + Fe cations													
Na (apfu)	7.080	6.810	6.712	6.786	6.749	6.654	6.802	6.951	6.551	6.443	6.496	6.484	6.513
Al	5.867	5.824	5.963	5.814	5.915	5.943	5.971	5.943	5.965	5.909	5.906	5.907	5.957
Si	6.132	6.118	6.037	6.165	6.085	6.057	6.029	6.057	6.028	6.063	6.091	6.093	6.04
S	0.886	0.87	0.752	0.741	0.552	0.547	0.541	0.554	0.447	0.426	0.451	0.426	0.447
K	0.125	0.135	0.089	0.158	0.027	0.026	0.027	0.026	0.015	0.016	0.017	0.016	0.012
Ca	0.383	0.365	0.631	0.626	0.825	0.817	0.82	0.828	1.032	1.025	1.015	1.012	1.017
Fe^{3+}	–	0.057	–	0.021	–	–	–	–	0.007	0.028	–	–	–
Sr	0.031	0.032	0.035	0.04	0.068	0.049	0.06	0.051	0.028	0.033	0.030	0.035	0.039
C*	0.19	0.06	0.33	0.48	0.77	0.69	0.77	0.84	0.91	0.89	0.9	0.92	0.89
A	7.62	7.34	7.47	7.61	7.67	7.55	7.71	7.86	7.63	7.52	7.56	7.55	7.58
Σ	1.08	0.93	1.09	1.22	1.32	1.23	1.31	1.40	1.36	1.32	1.35	1.34	1.34
Si:Al	1.05	1.05	1.01	1.06	1.03	1.02	1.01	1.02	1.01	1.03	1.03	1.03	1.01
(Na + K)/Ca	18.79	19.03	10.77	11.08	8.21	8.18	8.33	8.43	6.36	6.3	6.42	6.43	6.41
Mol.%	$Ccn_{6.5}$		$Ccn_{18.1}$	$Ccn_{24.5}$	$Ccn_{39.9}$		$Ccn_{42.3}$		$Ccn_{50.4}$	$Ccn_{50.5}$		$Ccn_{50.9}$	

Rock type	Vsh sye (leucocratic lenses)					Ccn-Nph sye				Ccn-Nph sye			
Sample no.	07-01 grain1			07-01 grain2		03-01 grain1		03-01 grain2		08-01 grain1		08-01 grain2	
Orientation	RO			⊥ *c* axis		RO		RO		⊥ *c* axis		RO	
Na_2O (wt.%)	19.79	19.99	20.41	20.43	20.24	18.50	18.23	17.90	18.56	18.50	18.61	17.77	17.68
Al_2O_3	29.72	29.74	29.69	29.71	29.58	29.51	29.21	29.86	29.66	29.27	29.30	29.69	29.40
SiO_2	35.59	36.52	36.93	36.25	36.21	36.13	35.58	35.71	35.60	35.89	35.94	36.29	35.92
SO_3	2.65	2.68	2.65	2.82	2.82	2.12	2.14	2.00	2.08	2.00	1.83	0.28	0.75
K_2O	0.07	0.06	0.08	0.09	0.08	0.04	0.06	0.04	0.05	0.03	0.05	0.03	0.06
CaO	4.81	4.78	4.66	4.75	4.77	7.23	7.01	7.26	7.08	6.87	7.23	8.24	7.87
Fe_2O_3	0.29	0.21	0.03	0.02	0.19	0.05	0.03	0.08	0.02	0.01	n.d.	0.02	n.d.
SrO	0.69	0.85	0.55	0.65	0.74	n.d.	0.11	0.10	n.d.	0.12	0.02	0.18	0.03
Total	93.61	94.83	95.00	94.72	94.63	93.58	92.37	92.95	93.05	92.69	92.98	92.50	91.71
Mineral formulae calculated on the basis of 12 Si + Al + Fe cations													
Na (apfu)	6.501	6.484	6.602	6.670	6.611	6.067	6.056	5.868	6.120	6.114	6.145	5.800	5.829
Al	5.934	5.864	5.837	5.896	5.875	5.882	5.899	5.951	5.945	5.881	5.881	5.890	5.892
Si	6.029	6.109	6.159	6.102	6.101	6.111	6.097	6.038	6.053	6.117	6.119	6.108	6.108
S	0.337	0.337	0.332	0.356	0.357	0.27	0.276	0.253	0.266	0.255	0.234	0.035	0.096
K	0.014	0.012	0.017	0.020	0.018	0.010	0.014	0.009	0.012	0.008	0.011	0.007	0.014
Ca	0.872	0.857	0.833	0.857	0.861	1.311	1.287	1.315	1.290	1.255	1.319	1.486	1.435
Fe^{3+}	0.037	0.026	–	–	0.024	0.007	–	0.011	–	–	–	–	–
Sr	0.067	0.083	0.053	0.063	0.073	–	0.010	0.010	–	0.012	–	–	–
C*	0.88	0.91	0.94	0.96	0.94	1.14	1.11	1.03	1.12	1.13	1.22	1.43	1.32
A	7.46	7.44	7.51	7.61	7.56	7.39	7.37	7.20	7.42	7.39	7.48	7.31	7.28
Σ	1.21	1.24	1.28	1.32	1.30	1.40	1.38	1.28	1.38	1.39	1.46	1.46	1.41
Si:Al	1.02	1.04	1.06	1.04	1.04	1.04	1.03	1.01	1.02	1.04	1.04	1.04	1.04
(Na + K)/Ca	7.47	7.58	7.94	7.80	7.70	4.64	4.72	4.47	4.75	4.88	4.67	3.91	4.07
Mol.%	$Ccn_{56.9}$			$Ccn_{57.7}$		$Ccn_{67.3}$		$Ccn_{67.4}$		$Ccn_{70.6}$		$Ccn_{91.3}$	

Cl was sought but not detected. Abbreviations: sye- syenite; apfu- atoms per formula unit; n.d. – not detected ; RO – random grain orientation; *C – carbon content calculated based on charge balance; *A* = Na+K+Ca+Sr; Σ= $(CO_3)^{2-}$ + $(SO_4)^{2-}$

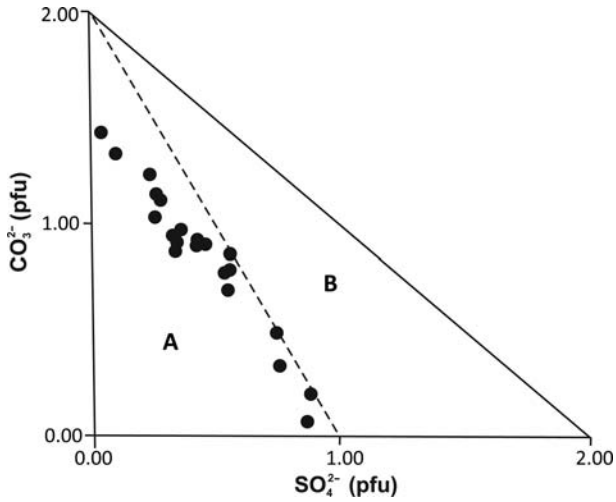

FIG. 3. Cinder Lake samples plot in the area for non-stoichiometric compositions (A). The dashed line indicates the ideal solid solution between cancrinite and vishnevite. Area B indicates complex stacking sequences in the crystal structure; discrimination diagram after Hassan and Grundy (1984).

K_2O (≤0.1 wt.%). Strontium is a nearly ubiquitous substituent in the material examined, and tends to occur in elevated concentrations (0.3–0.8 wt.% SrO) in relatively vishnevite-rich grains (<60% Ccn). The more Ca-rich members of the series contain ≤0.1 wt.% SrO. No clear correlation is observed among the substituent elements and Na (or Ca) across our sample suite, evidently because of their very different crystallization conditions.

Raman spectroscopy

Representative Raman spectra of the samples approaching the cancrinite and vishnevite end-members, as well as an example with an intermediate composition, are given in Fig. 5 and the measured Raman shifts are summarized in Table 2.

Peaks below 500 cm^{-1} (84–98, 196–198, 230–233, 269–276, 289–299, 335–342; 402–404; 440–442, 464–466 and 513–520 cm^{-1}) are interpreted to be deformational modes of the aluminosilicate framework νδO–Si(Al)–O and (Na–Ca)–O modes (Fig. 5*a*,*b*,*c*; Reshetnyak *et al*., 1988; Gatta *et al*., 2012). We did not observe any significant changes in these vibration modes across our sample suite, owing to their similar Al and Si contents (see Table 1). Less-intense peaks observed in the range 630 to 720 cm^{-1} appear to depend on the concentrations of SO_4^{2-} and CO_3^{2-}. The 631–633 cm^{-1} peak, corresponding to the $\nu_4(SO_4)$ mode, is more predominant in cancrinite-poor compositions (Fig. 5*a*,*b*) and the 718–720 cm^{-1} peak correlates well with the CO_3^{2-} vibration mode (ν_4) in cancrinite-rich compositions (Fig. 5*c*; Gunasekaran *et al*., 2006; Gatta *et al*., 2012). The most intense Raman peaks at 984–992 and 1046–1060 cm^{-1} can be interpreted as the stretching modes of SO_4^{2-} and CO_3^{2-} ions, respectively (Reshetnyak *et al*., 1988). According to these authors, their high intensity by comparison with the low wavenumber framework signals is due to the higher polarizability of CO_3^{2-} and SO_4^{2-} relative to SiO_4^{4-} and AlO_4^{5-} groups. From $Ccn_{91.36}$ towards $Ccn_{6.5}$, we observe the gradual disappearance of the carbonate modes at 686–774 cm^{-1} (interpreted as in-plane bending modes of carbonate groups; Gatta *et al*., 2012) and 1046–1060 cm^{-1} (interpreted as symmetric stretching modes of carbonate groups; Gatta *et al*., 2012). An additional SO_4^{2-} signal is observed in sample $Ccn_{6.5}$ at 984 cm^{-1} and is tentatively identified as the $\nu_1(A_1)$ symmetric mode (Reshetnyak *et al*., 1988; Fig. 5*a*). The peak at 1056 cm^{-1} is interpreted as a minor contribution of the CO_3^{2-} group as this sample has 1.33–1.22 C apfu (Table 1). Peaks characteristic of both CO_3^{2-} and SO_4^{2-} are shown in Fig. 5*b* (sample $Ccn_{70.6}$), as expected from its intermediate composition.

Using *LabSpec* software (Horiba Scientific), the O–H stretching vibrations can be deconvoluted into at least two components centred at ~3540–3547 and 3586–3591 cm^{-1}, consistent with the O–H stretching range for H_2O in the cancrinite–vishnevite series (Reshetnyak *et al*., 1988; Della Ventura *et al*.,

https://doi.org/10.1180/minmag.2016.080.165 Published online by Cambridge University Press

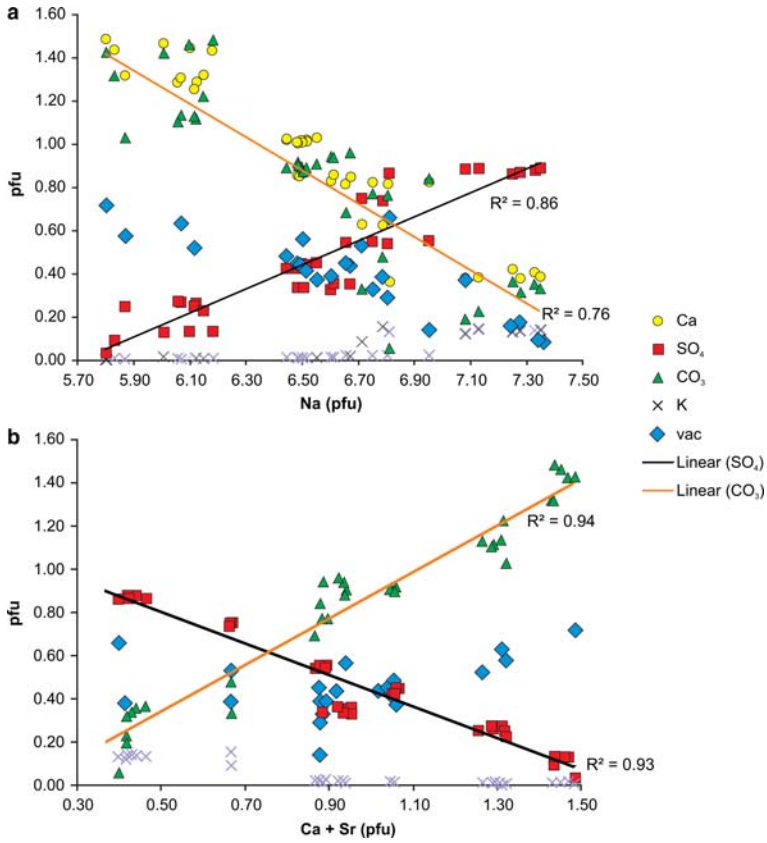

FIG. 4. Distribution of selected elements in cancrinite–vishnevite series from Cinder Lake as a function of (*a*) Na and (*b*) (Ca + Sr) content. Linear correlations and correlation coefficients are shown for SO_4^{2-} and CO_3^{2-}. All values are per formula unit (pfu).

2007, 2009). The 3591 cm^{-1} peak (antisymmetric vibration mode) is not observed in the cancrinite-poor members of the series studied, which could be due to changes in the symmetry of H_2O molecule in response to the CO_3^{2-}/SO_4^{2-} substitution in the channels (G. Della Ventura, pers. comm.). We did not observe any peaks in the region from 1200 to 3400 cm^{-1} that could be attributed to unaccounted water species in the structural channels (Della Ventura *et al*., 2007).

X-ray microdiffraction

In order to determine whether microbeam X-ray methods can be used reliably to discriminate among the members of the cancrinite–vishnevite series, diffraction data were collected *in situ* for the Cinder Lake samples and compared with those in the literature. Because end-member compositions have been studied in detail by previous workers (Grundy and Hassan, 1982; Hassan *et al*., 2006; Della Ventura *et al*., 2007), we focused on less-studied intermediate members of the series in the present work. The measured patterns show strong ($I \geq 8$) peaks at 3.22–3.24 Å (121) and 2.56–2.58 Å (002), characteristic of both cancrinite and vishnevite. The relative positions of these and other lines shift to lower *d* values with increasing cancrinite content (Table 3 and Supplementary Data which has been deposited with the Principal Editor of *Mineralogical Magazine* and is available from http://www.minersoc.org/pages/e_journals/dep_mat_mm.html). Cancrinite 03-01 ($Ccn_{70.6}$) is the only sample showing a weak diffraction line which could indexed as (1.1.13), and is indicative of a supercell (Hassan *et al*., 2006). It is observed in both perpendicular (with respect to [0001]) and random orientations. The (016) superlattice peak

https://doi.org/10.1180/minmag.2016.080.165 Published online by Cambridge University Press

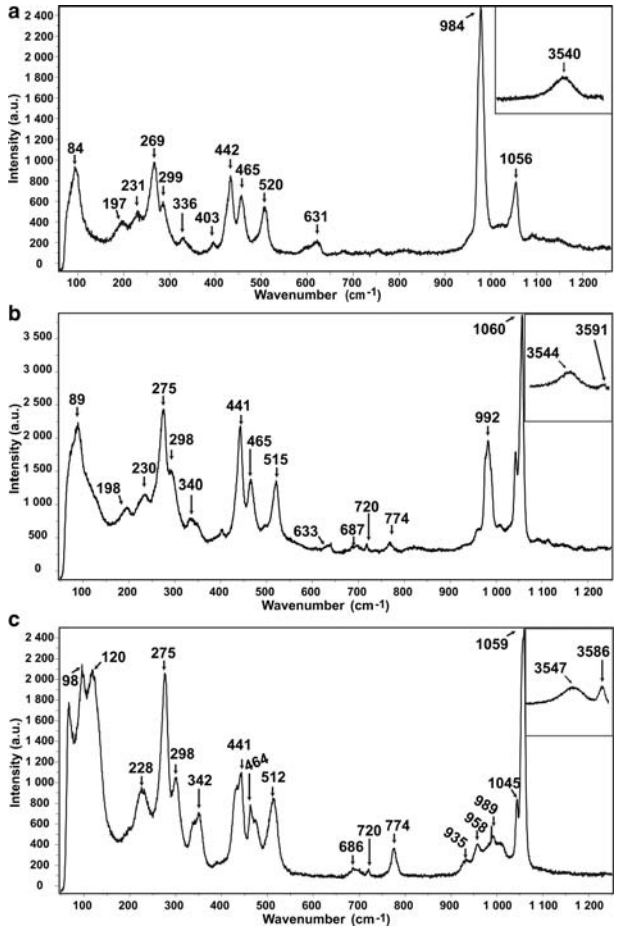

FIG. 5. Representative Raman spectra for: (*a*) $Ccn_{6.5}$ (sample 04-01); (*b*) $Ccn_{70.6}$ (sample 07-01); and (*c*) $Ccn_{91.3}$ (sample 08-01) in Fig. 2. Insets show the O–H stretching range (2750 to 3600 cm^{-1}); a.u. = arbitrary units.

TABLE 2. Representative Raman modes (cm^{-1}) of cancrinite-group minerals from Cinder Lake.

Vibrational modes (cm^{-1})	This study		Reshetnyak *et al.* (1988)		Gatta *et al.* (2012)
	$Ccn_{6.5}$	$Ccn_{91.36}$	Cancrinite	Vishnevite	Cancrinite
CO_3^{2-}	n/o*	633; 687	n/o	n/o	631–685
Activation modes	n/o	720; 774	720–772	n/o	768–816
	n/o	935; 958; 989	933; 960	n/o	938–1057
	n/o	1045; 1059	1043–1058	n/o	n/o
	n/o	n/o	1388–1520	n/o	n/o
SO_4^{2-}	631	n/o	n/o	630	n/a*
Activation modes	984	n/o	n/o	996	n/a*
	n/o	n/o	n/o	1140	n/a*
H_2O	3540	3547	3540	3530	3536
Activation modes	n/o	3586	3585	3590	3647

*Abbreviations: n/o – not observed; n/a – not applicable

https://doi.org/10.1180/minmag.2016.080.165 Published online by Cambridge University Press

TABLE 3. Micro-XRD pattern of samples 08-01 ($Ccn_{70.6}$) and 04-01 ($Ccn_{6.5}$). Both measurements were performed perpendicular to the *c* axis.

$Ccn_{70.6}$						$Ccn_{6.5}$					
h	*k*	*l*	*d*(obs)	*d*(calc)	*I*	*h*	*k*	*l*	*d*(obs)	*d*(calc)	*I*
1	0	1	4.655	4.651	16	1	0	1	4.677	4.679	77
2	1	0	4.143	4.131	1	2	1	0	4.158	4.145	2
1	1	1	3.981	3.985	1	1	1	1	3.997	4.006	1
2	0	1	3.748	3.744	2	2	0	1	3.762	3.763	1
3	0	0	3.661	3.643	5	3	0	0	3.672	3.656	1
1	2	1	3.220	3.22	100	1	2	1	3.241	3.235	100
1	3	0	3.046	3.031	1	1	3	0	3.046	3.042	2
3	0	1	2.966	2.972	5	3	0	1	2.992	2.985	2
4	0	0	2.744	2.732	10	4	0	0	2.740	2.742	4
1	3	1	2.614	2.611	19	1	3	1	2.620	2.622	17
0	0	2	2.569	2.570	35	0	0	2	2.585	2.586	87
2	3	0	2.508	2.507	5	1	0	2	2.520	2.517	16
1	0	2	2.499	2.502	5	4	0	1	2.419	2.423	23
4	0	1	2.419	2.413	18	1	4	0	2.394	2.393	11
1	4	0	2.381	2.385	2	0	2	2	2.334	2.339	3
0	2	2	2.326	2.326	1	3	2	1	2.260	2.263	12
3	2	1	2.252	2.254	10	0	5	0	2.194	2.193	7
0	5	0	2.186	2.186	2	1	4	1	2.170	2.172	8
2	1	2	2.181	2.182	1	3	3	0	2.111	2.111	38
1	4	1	2.164	2.164	6	5	0	1	2.016	2.019	6
3	3	0	2.104	2.103	6	2	2	2	2.005	2.003	5
3	0	2	2.100	2.100	25	5	1	0	1.971	1.970	4
5	0	1	2.012	2.012	5	2	4	1	1.924	1.924	2
2	2	2	1.998	1.993	1	4	0	2	1.881	1.881	23
1	5	0	1.963	1.963	2	1	5	1	1.838	1.841	2
2	4	1	1.915	1.917	1	3	2	2	1.802	1.803	20
4	0	2	1.873	1.872	23	2	5	0	1.756	1.756	16
1	5	1	1.837	1.834	1	0	6	1	1.721	1.723	1
3	2	2	1.795	1.795	19	4	3	1	1.702	1.703	14
2	5	0	1.749	1.750	10	5	0	2	1.672	1.673	2
1	4	2	1.745	1.748	2	2	5	1	1.662	1.663	4
0	6	1	1.716	1.717	1	2	0	3	1.645	1.645	10
4	3	1	1.696	1.696	3	3	3	2	1.635	1.635	4
1	0	3	1.692	1.693	5	4	2	2	1.617	1.617	1
5	0	2	1.666	1.665	2	2	1	3	1.592	1.592	30
2	5	1	1.656	1.657	2	4	4	0	1.583	1.583	5
2	0	3	1.635	1.635	6	5	3	0	1.566	1.567	2
3	3	2	1.627	1.628	2	3	0	3	1.559	1.560	2
4	2	2	1.610	1.61	1	5	3	1	1.500	1.499	25
2	1	3	1.582	1.583	24	0	6	2	1.493	1.493	10
4	4	0	1.578	1.578	14	4	3	2	1.479	1.479	3
5	3	0	1.561	1.561	3	0	4	3	1.459	1.460	20
5	3	1	1.493	1.494	14	1	7	0	1.453	1.453	13
1	3	3	1.491	1.492	2	3	2	3	1.423	1.422	6
0	6	2	1.487	1.486	7	6	1	2	1.405	1.404	1
4	3	2	1.473	1.473	2	3	6	0	1.382	1.382	1
0	4	3	1.451	1.452	16	8	0	0	1.370	1.371	4
1	7	0	1.448	1.448	14	4	5	1	1.355	1.355	2
3	2	3	1.414	1.415	4	4	4	2	1.350	1.350	13
3	6	0	1.377	1.377	1	5	3	2	1.340	1.340	4

(continued)

https://doi.org/10.1180/minmag.2016.080.165 Published online by Cambridge University Press

TABLE 3. (*contd*.)

$Ccn_{70.6}$						$Ccn_{6.5}$					
h	*k*	*l*	*d*(obs)	*d*(calc)	*I*	*h*	*k*	*l*	*d*(obs)	*d*(calc)	*I*
4	4	2	1.345	1.344	6	0	8	1	1.325	1.325	12
5	3	2	1.335	1.334	2	1	5	3	1.298	1.297	9
0	8	1	1.320	1.320	5	0	0	4	1.294	1.293	9
2	4	3	1.320	1.319	2	1	7	2	1.267	1.267	13
1	5	3	1.291	1.291	2	4	6	0	1.258	1.258	2
0	0	4	1.285	1.285	4	1	8	1	1.246	1.246	7
1	7	2	1.261	1.261	10	3	6	2	1.219	1.219	10
1	1	4	1.259	1.259	9	0	8	2	1.211	1.211	2
4	6	0	1.251	1.254	1	7	3	1	1.201	1.200	3
1	8	1	1.241	1.241	2	4	0	4	1.169	1.170	4
4	3	3	1.240	1.240	3	0	7	3	1.160	1.160	5
3	6	2	1.214	1.214	6	2	3	4	1.150	1.150	4
0	8	2	1.207	1.206	1	2	6	3	1.141	1.141	11
7	3	1	1.196	1.196	1	4	6	2	1.131	1.131	2
2	8	0	1.193	1.193	1	5	6	1	1.122	1.122	1
2	2	4	1.190	1.190	2	0	9	2	1.103	1.102	1
0	4	4	1.164	1.163	1	3	8	1	1.089	1.089	1
8	2	1	1.163	1.162	1						
0	7	3	1.154	1.154	5						
6	5	0	1.145	1.146	1						
2	3	4	1.143	1.144	2						
2	6	3	1.135	1.135	2						
4	7	0	1.133	1.133	2						
4	6	2	1.126	1.127	0						
5	6	1	1.118	1.118	1						
0	9	2	1.098	1.098	1						

also identified by Hassan *et al*. (2006) occurs at too low an angle to be observed in our measurements.

The patterns of the Cinder Lake samples can be indexed on the basis of a hexagonal unit cell (space group $P6_3$); the calculated cell parameters range from a = 12.664(1) Å and c = 5.173(1) Å for vishnevite Ccn_{22} to a = 12.613(1) Å and c = 5.132(1) Å for cancrinite Ccn_{71}. These values are in good agreement with those reported by previous workers (Grundy and Hassan, 1982; Hassan *et al*. 2006; Della Ventura *et al*., 2007; Pekov *et al*., 2011). Both cell parameters decrease with increasing cancrinite content (Fig. 6*a*,*b*). A complete dataset of μXRD results can be found in the Supplementary material at http://www.minersoc.org/pages/e_journals/dep_mat_mm.html.

Discussion and conclusions

The cancrinite–vishnevite solid solution present at Cinder Lake ranges in composition from $Ccn_{6.5}$ to $Ccn_{91.3}$ (Table 1). The observed compositional variation cannot be adequately represented by a single substitution scheme. From Figs 3 and 4, it is clear that the carbonate-for-sulphate substitution [$2CO_3^{2-} \leftrightarrow SO_4^{2-}$] is compensated, to a large extent, by the loss of charge at the Na2 site where Ca^{2+} is concomitantly replaced by Na^+ (see section on Background information). There is also a less well-defined but detectable increase in the number of vacancies in the large cation sites with decreasing SO_4^{2-} content (Fig. 4), implying the following alternative coupled substitution: Ca^{2+} + [vac] + $CO_3^{2-} \leftrightarrow$ 2 Na^+ + SO_4^{2-}. The two mechanisms operate in conjunction, and the most Ca-rich members in our sample suite approach the theoretical cation-deficient composition $Na_6Ca\square(Al_6Si_6O_{24})(CO_3)\cdot nH_2O$ (□ = vacancy). Other large cations are present at low levels (<0.2 apfu total) and are not expected to have any significant effect on the spectroscopic or structural parameters. The compositions examined tend to have a higher Si:Al ratio than the stoichiometric value of one. The

https://doi.org/10.1180/minmag.2016.080.165 Published online by Cambridge University Press

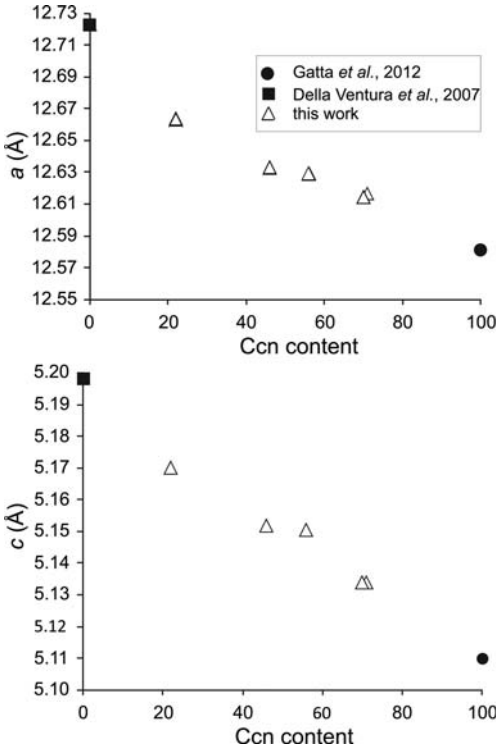

FIG. 6. Variation in unit-cell parameters across the cancrinite–vishnevite series (this work and data from the literature).

deviation is small, however, and does not seem to affect the framework deformation modes in their Raman spectra (see above).

The chemical variation of the studied cancrinite-group minerals is reflected in their Raman spectra. It is clear from our results that the positions of Raman peaks change systematically with their cancrinite content (Fig. 5). For example, sample $Ccn_{91.3}$ yields most of the peaks characteristic of the CO_3^{2-} vibration modes identified by Reshetnyak *et al*. (1988); in contrast, composition $Ccn_{6.5}$ shows mostly the SO_4^{2-} modes. Raman spectroscopy has proven to be an excellent non-destructive express technique that can be used for the identification of small (<30 μm) grains of cancrinite–vishnevite feldspathoids in thin section. It can be used to identify the presence of CO_3^{2-} groups and H_2O, and potentially quantify the proportion of CO_3^{2-} with respect to SO_4^{2-}, if a suitable set of standards were developed. Chemical variations across the cancrinite–vishnevite series can also be tracked from the unit-cell parameters or, in the first approximation, from interplanar distances of the major diffraction lines (Table 3, Fig. 6).

The study of cancrinite-group minerals is important for ascertaining the nature and activity of volatile species (CO_2, SO_3, H_2O) in igneous systems. In particular, cancrinite-dominant compositions are believed to indicate a high $P(CO_2)$ in the melt/fluid (Pekov *et al*., 2011). Vishnevite does not only imply the enrichment of its parental liquid in S, but also points to oxidizing conditions. These minerals can also be used to track petrogenetic evolution of alkaline magmas (Coulson *et al*., 1999; Dawson *et al*., 1995; Chukanov *et al*., 2010; Cordier *et al*., 2005). At Cinder Lake, we recognize a wide range of compositions from vishnevite to cancrinite, which is unparalleled by any other alkaline locality in the world. Cancrinite here occurs as a primary major constituent interstitial with respect to feldspars and biotite, or as a late-stage mineral replacing nepheline, whereas vishnevite occurs interstitially in association with calcite, potassium feldspar and biotite (see section on Petrography). The order of emplacement of these feldspathoid syenites is interpreted to be from cancrinite-nepheline syenite to vishnevite syenite (Kressall, 2012). This progression is accompanied by an increasing degree of silica-undersaturation along with increasing enrichment of the parental phonolitic magma in CaO, MgO, $(Fe_2O_3)_{TOTAL}$, P_2O_5, TiO_2, SrO, BaO, REE_2O_3, CO_2, F and SO_3, and its depletion in Na_2O, K_2O and Al_2O_3 in the course of magma evolution (Kressall, 2012). The observed textural relations indicate that the late-stage cancrinite formed as a reaction product between euhedral nepheline and a CO_2-bearing residual liquid (Fig. 2*b*), providing further support to the importance of late-magmatic processes in the evolution of the Cinder Lake alkaline suite (cf. Cordier *et al*., 2005). The abundance of sulfate-bearing feldspathoids and absence of primary pyrrhotite at Cinder Lake indicate oxidizing conditions above the NNO buffer (Baudouin and Parat, 2015). The compositional variation of cancrinite indicates that in the leucocratic cancrinite-nepheline syenite, the residual melt was significantly enriched in Ca and CO_3^{2-} relative to Na and SO_4^{2-} in comparison with the clinopyroxene-bearing cancrinite-nepheline syenite. Vishnevite does not occur as a reaction product here, forming instead late-stage interstitial intergrowths with albite and calcite. An increase in CO_2 concentrations and decrease in SiO_2 with magma evolution is also reflected in the high modal proportion of

https://doi.org/10.1180/minmag.2016.080.165 Published online by Cambridge University Press

Sr-rich calcite in the vishnevite syenite. Evidently, the build-up of CO_2 in this case does not result in precipitation of cancrinite, but triggers deposition of calcite and sequestration of SO_3 and Na by vishnevite. This example shows that the presence of the latter mineral alone is not necessarily indicative of low $P(CO_2)$. At high Ca activity, carbonate will partition preferentially into calcite, rather than feldspathoid minerals. A build-up of CO_2 and other volatiles with magma evolution is observed at other localities of alkaline rocks such as the Grønnedal- Íka complex in Greenland (Bedford, 1989) and the Sung Valley alkaline-carbonatite complex in India (Melluso *et al*., 2010).

Acknowledgements

This work was supported by a postdoctoral fellowship (awarded to TM) from Fundação para a Ciência e a Tecnologia, Portugal (SFRH/BPD/62915/2009) with EU and Portuguese funds (POPH- QREN), and the Natural Sciences and Engineering Research Council of Canada (Discovery grant to ARC and Graduate Scholarship to RDK). We also appreciate the logistic and support in-kind from the Manitoba Geological Survey. The help of Panseok Yang and Ravinder Sidhu (University of Manitoba) with electron microprobe analysis, and of Bonnie Lenton (Manitoba Geological Survey) with figure preparation is gratefully acknowledged. We also acknowledge G. Diego Gatta, Fernando Cámara and Giancarlo Della Ventura for their constructive and detailed comments on the earlier version of this paper, and Giancarlo Della Ventura for editorial handling.

References

Barney, G.S. (1976) Fixation of radioactive waste by hydrothermal reaction with clays. *Advances in Chemistry*, **153**, 108–125.

Baudouin, C. and Parat, F. (2015) Role of volatiles (S, Cl, H_2O) and silica activity on the crystallization of haüyne and nosean in phonolitic magmas (Eifel, Germany and Saghro, Morocco). *American Mineralogist*, **100**, 2308–2322.

Bedford, C.M. (1989) *The Mineralogy, Geochemistry, and Petrogenesis of the Grønnedal- Íka Alkaline Igneous Complex, south-west Greenland*. PhD Theses, Durham University, UK.

Cordier, C., Clémont, J.P., Caroff, M., Hémond C., Blais, S. Cotten, J., Bollinger, C. Launeau, P. and Guille, G. (2005) Petrogenesis of coarse-grained intrusives from Tahiti Nui and Raiatea (Society Islands, French Polynesia). *Journal of Petrology*, **46**, 2281–2312.

Corkery, M.T., Cameron, H.D.M., Lin, S., Skulski, T., Whalen, J.B. and Stern, R.A. (2000) Geological investigations in the Knee Lake belt (parts of NTS 53L); Pp. 129–136 in: *Report of Activities 2000.* Manitoba Industry, Trade and Mines, Manitoba Geological Survey, Canada.

Coulson, I.M., Russell, J.K. and Dipple, G.M. (1999) Origins of the Zippa Mountain pluton: a Late Triassic, arc-derived, ultrapotassic magma from the Canadian Cordillera. *Canadian Journal of Earth Sciences*, **36**, 1415–1434.

Chakhmouradian, A.R., Böhm, C.O., Kressall, R.D. and Lenton, P.G. (2008) Evaluation of the age, extent and composition of the Cinder Lake alkaline intrusive complex, Knee Lake area, Manitoba (part of NTS 53L15). Pp. 109–120 in: *Report of Activities 2008.* Manitoba Science, Technology, Energy and Mines, Manitoba Geological Survey, Canada.

Chukanov, N.V., Pekov. I.V., Olysych, L.V, Massa, W., Yakubovich, O.V., Zadov, A.E., Rastsvetaeva, R.K. and Vigasi, M.F. (2010) Kyanoxalite, a new cancrinite-group mineral species with extraframework oxalate anion from the Lovozero alkaline pluton, Kola Peninsula. *Geology of Ore Deposits*, **52**, 778–790.

Chukanov, N.V., Pekov, I.V., Olysych, L.V, Zubkova, N.V. and Vigasina, M.F. (2011) Crystal chemistry of cancrinite-group minerals with an AB-type framework: a review and new data. II. IR Spectroscopy and its crystal chemical implications. *The Canadian Mineralogist*, **49**, 1151–1164.

Dawson, J.B., Smith, J.V. and Steele, I.M. (1995) Petrology and mineral chemistry of plutonic igneous xenoliths from the carbonatite volcano, Oldoinyo Lengai, Tanzania. *Journal of Petrology*, **36**, 797–826.

Deer, W.A., Howie, R.A. and Zussman, J. (1992) *An Introduction to The Rock Forming Minerals*. 2nd Ed., Pearson Education Limited, Harlow, UK.

Della Ventura, G. and Bellatreccia, F. (2004) The channel constituents of cancrinite-group minerals. Pp. 75–76 in: *Proceedings Micro- and Mesoporous Mineral Phases.* Accademia Nazionale dei Lincei, Rome, Italy.

Della Ventura, G., Bellatreccia, F. and Bonaccorsi, E. (2005) CO_2 in minerals of the cancrinite-sodalite group: pitiglianoite. *European Journal of Mineralogy*, **17**, 847–851.

Della Ventura, G., Bellatreccia, F., Parodi, G.C., Cámara, F. and Piccinini, M. (2007) Single-crystal FTIR and X-ray study of vishnevite, ideally $[Na_6(SO_4)][Na_2(H_2O)_2][Si_6Al_6O_{24}]$. *American Mineralogist*, **92**, 713–721.

Della Ventura, G.D., Bellatreccia, F. and Piccinini, M. (2008) Channel CO_2 in feldspathoids: new data and new perspectives. *Rendiconti Lincei*, **19**, 141–159.

Della Ventura, G., Gatta, D., Redhammer, G., Bellatreccia, F., Loose, A. and Parodi, G.C. (2009) Single-crystal

https://doi.org/10.1180/minmag.2016.080.165 Published online by Cambridge University Press

polarized FTIR spectroscopy and neutron diffraction refinement of cancrinite. *Physics and Chemistry of Minerals*, **36**, 193–206.

Dumańska-Słowik, M., Pieczka, A. Heflik, W. and Sikorska, M. (2016) Cancrinite from nepheline (mariupolite) of the Oktiabrski massif, SE Ukraine, and its growth history. *Spectrochimica Acta Part A: Molecular and Biomolecular Spectroscopy*, **157**, 211–219.

Gatta, G.D. and Lee, Y. (2008) Pressure-induced structural evolution and elastic behaviour of $Na_6Cs_2Ga_6Ge_6O_{24}{\cdot}Ge(OH)_6$ variant of cancrinite: a synchrotron powder diffraction study. *Microporous and Mesoporous Materials*, **116**, 51–58.

Gatta, G.D. and Lotti, P. (2016) Cancrinite-group minerals: crystal-chemical description and properties under non-ambient conditions – a review. *American Mineralogist*, **101**, 253–265.

Gatta, G.D., Lotti, P., Kahlenberg, V. and Haefeker, U. (2012) The low-temperature behaviour of cancrinite: an *in situ* single-crystal X-ray diffraction study. *Mineralogical Magazine*, **76**, 933–948.

Gatta, G.D., Comboni, D., Alvaro, M., Lotti, P., Cámara, F. and Domeneghetti, M.C. (2014) Thermoelastic behavior and dehydration process of cancrinite. *Physics and Chemistry of Minerals*, **41**, 373–386.

Gilbert, H.P. (1985) Geology of Knee-Lake-Gods Lake area. *Manitoba Energy and Mines, Geological Services, Geological Report*, GR83–1B. Manitoba, Canada.

Grundy, H.D. and Hassan, I. (1982) The crystal structure of carbonate-rich cancrinite. *The Canadian Mineralogist. 20*, 239–251.

Gunasekaran, S., Anbalagan, G. and Pandi, S. (2006) Raman and infrared spectra of carbonates of calcite structure. *Journal of Raman Spectroscopy*, **37**, 892–899.

Hassan, I. (1996*a*) Thermal expansion of cancrinite. *Mineralogical Magazine*, **60**, 949–956.

Hassan, I. (1996*b*) The thermal behavior of cancrinite. *The Canadian Mineralogist*, **34**, 893–900.

Hassan, I. and Buseck, P.R. (1992) The origin of the superstructure and modulations in cancrinite. *The Canadian Mineralogist*, **30**, 49–59.

Hassan, I. and Grundy, H.D. (1984) The character of the cancrinite-vishnevite solid-solution series. *The Canadian Mineralogist*, **22**, 333–340.

Hassan, I. and Grundy, H.D. (1991) The crystal structure of basic cancrinite, ideally $Na_8[Al_6Si_6O_{24}](OH)_2{\cdot}3H_2O$. *The Canadian Mineralogist*, **29**, 377–383.

Hassan, I., Antao, S.M. and Parise, J.B. (2006) Cancrinite: crystal structure, phase transitions, and dehydration behavior with temperature. *American Mineralogist*, **91**, 1117–1124.

Holland, T.J.B. and Redfern, S.A.T. (1997) UNITCELL: a nonlinear least-squares program for cell-parameter refinement and implementing regression and deletion diagnostics. *Journal of Applied Crystallography*, **30**, 84.

Horváth, L. and Gault, R.A. (1990) The mineralogy of Mont Saint-Hilaire, Quebec. *Mineralogical Record*, **21**, 281–359.

Hubregtse, J.J.M.W. (1985) Geology of the Oxford Lake–Carrot River area. *Manitoba Energy and Mines, Geological Services, Geological Report*, GR83–1A. Manitoba, Canada.

Kressall, R. (2012) *The Petrology, Mineralogy and Geochemistry of the Cinder Lake Alkaline Intrusive Complex, Eastern Manitoba*. MSc thesis, University of Manitoba, Canada.

Lin, S., Davis, D.W., Rotenberg, E., Corkery, M.T. and Bailes, A.H. (2006) Geological evolution of the northwestern Superior Province: clues from geology, kinematics, and geochronology in the Gods Lake Narrows area, Oxford–Stull terrane, Manitoba. *Canadian Journal of Earth Sciences*, **43**, 749–765.

Lotti, P., Gatta, G.D., Rotiroti, N. and Cámara, F. (2012) High-pressure study of a natural cancrinite. *American Mineralogist*, **97**, 872–882.

Lotti, P., Gatta, G.D., Merlini, M. and Hanfland, M. (2014*a*) High-pressure behavior of davyne [CAN-topology]: An in situ single-crystal synchrotron diffraction study. *Microporous and Mesoporous Materials*, **198**, 203–214.

Lotti, P., Gatta, G.D., Rotiroti, N., Cámara, F. and Harlow, G.E. (2014*b*) The high-pressure behavior of ballirianoite: a cancrinite group mineral. *Zeitschrift für Kristallogrophie*, **229**, 63–76.

Melluso, L., Srivastava, R.K., Guarino, V., Zanetti, A. and Sinha, A.K. (2010) Mineral compositions and petrogenetic evolution of the ultramafic-alkaline-carbonatitic complex of Sung Valley, Northeastern India. *The Canadian Mineralogist*, **48**, 205–229.

Olysych, L.V., Pekov, I.V. and Agakhanov, A.A. (2008) Chemistry of cancrinite-group minerals from the Khibiny-Lovozero alkaline complex, Kola Peninsula, Russia. Pp. 91–94: *Minerals as Advanced Materials I*. Springer Berlin Heidelberg, Germany.

Pekov, I.V., Olysych, L.V., Chukanov, N.V., Zubkova, N. V., Pushcharovsky, D.Y., Van, V.K., Giester, G. and Tillmanns, E. (2011) Crystal chemistry of cancrinite-group minerals with an AB-type framework: a review and new data. I. Chemical and structural variations. *The Canadian Mineralogist*, **49**, 1129–1150.

Phoenix, R. and Nuffield, E.W. (1949) Cancrinite from Blue Mountain, Ontario. *American Mineralogist*, **34**, 452–455.

Pouchou, J.L. and Pichoir, F. (1985) "PAP" (φ-ρ-Z) correction procedure for improved quantitative microanalysis. Pp. 104–106 in: *Microbeam Analysis* (J.T. Armstrong, editor). San Francisco Press, San Francisco, USA.

Rastsvetaeva, I.V., Pekov, I.V., Chukanov, N.V., Rozenberg, K.A. and Olysych, L.V. (2007) Crystal structures of low-symmetry cancrinite and cancrisilite varieties. *Crystallography Reports*, **52**, 811–818.

https://doi.org/10.1180/minmag.2016.080.165 Published online by Cambridge University Press

Reshetnyak, N.B., Sosedko, T.A. and Tret'yakova, L.I. (1988) Combination light scattering in minerals. *Mineralogicheskii Zhurnal*, **10**, 69–73.

Stott, G.M., Corkery, M.T., Percival, J.A., Simard, M. and Goutier, J. (2010) A revised terrane subdivision of the Superior Province. *Ontario Geological Survey, Open File Report*, **6260**, 20-1–20-10. Ontario, Canada.

Wright, J.F. (1932) Oxford House area, Manitoba. *Canada Department of Mines, Geological Survey Summary Report*, **1931 (C)**, 1C–25C.

https://doi.org/10.1180/minmag.2016.080.165 Published online by Cambridge University Press